Hindawi
Shock and Vibration
Volume 2022, Article ID 3640268, 13 pages
https://doi.org/10.1155/2022/3640268

Research Article

Cooperative Control of Interconnected Air Suspension Based on Energy Consumption Optimization

Guoqing Geng,[1] Shuai Zeng ,[1] Liqin Sun ,[1] Zhongxing Li,[1] and Wenhao Yu[2]

[1]*School of Automobile and Traffic Engineering, Jiangsu University, Zhenjiang 212013, China*
[2]*School of Vehicles and Transportation, Tsinghua University, Beijing 100084, China*

Correspondence should be addressed to Liqin Sun; slq@ujs.edu.cn

Received 15 April 2021; Revised 29 November 2021; Accepted 22 February 2022; Published 6 April 2022

Academic Editor: Marcos Silveira

In this study, a cooperative control method based on model predictive control and multiagent theory is proposed to control an interconnected air suspension system with three controllable structures of interconnection mode, damping, and vehicle height. The model predictive controller is constructed based on a discrete-time state-space model. The optimal interval for suspension force is obtained through solving cost functions while satisfying a set of constraints on controlled variables and thereby reducing the coupling complexity of a multivariable control system. Deliberative agents are involved in building cost functions of interconnection mode, vehicle height adjustment, and damping force, and the energy consumption control strategy is established to realize suspension force distribution with low energy consumption. Finally, the test results show that the proposed control method can significantly improve vehicle ride comfort and restrain rollover on the premise of ensuring energy efficiency. Compared with traditional control, the peak value of the sprung mass acceleration speed decreases by 70% and the peak value of the unsprung mass acceleration speed decreases by 75% under straight-driving condition. The roll angle decreases by 40% under the steering condition. As for the traditional control, they are skyhook, imitation skyhook, and PID-PWM control strategies.

1. Introduction

Air suspension with adjustable spring stiffness and good vibration isolation can help improve vehicle ride comfort. Thus, more and more automobiles are equipped with an air suspension system [1]. Such excellent performance has attracted scholars to make a deep study on the height control and damping characteristics [2, 3]. To further improve the comprehensive performance of air suspension, Higginbotham proposed a new structure of interconnected air suspension system (IASS) [4]. Bhave built a longitudinal interconnected air suspension model and verified its accuracy [5]. Interconnected air suspension can help improve vehicle ride comfort and road friendliness [6]. Advantages of IASS make it widely used in sport utility vehicles such as the third-generation Range Rover (L322) [7]. The research group has carried out relevant research and built the corresponding test platform since 2014 [8, 9].

The IASS, as shown in Figure 1, is mainly composed of four air springs, four adjustable dampers, four air pressure sensors, four height sensors, four solenoid valves, interconnected pipelines, a gas tank, and an electronic control unit (ECU). Based on the traditional air suspension system, the adjacent air springs in IASS are connected by pipelines [10]. When an air spring is impacted due to uneven road surface, the interconnected pipeline makes the gas exchange between the air springs, so that the interconnected air spring can jointly bear the local road impact, to alleviate the road impact and improve the tire grounding and road friendliness. When the vehicle is accelerated or decelerated or subjected to large lateral force, the interconnection can be closed through the interconnection solenoid valve to ensure the vehicle handling stability. So in the study, the four-corner interconnected air suspension is considered as the research object and four solenoid valves are in open states.

IASS includes three controllable structures: interconnection mode, vehicle height, and damping. Typically, the

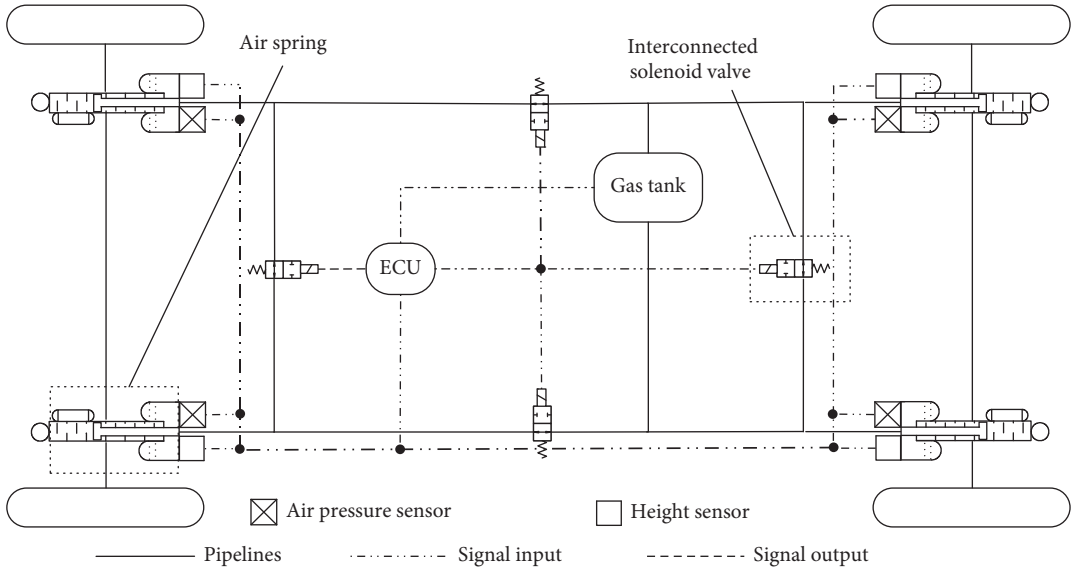

Figure 1: Structure of the four-corner interconnected air suspension.

three controllable structures are correlated, making the coupled system too complex to be applied with traditional cooperative control. In 2013, Wang proposed a multimode switching control method of body height and damping based on adjusting body height [11]. In 2014, Sun proposed an interconnection and damping hierarchical control method based on interconnected air suspension [12]. In the same year, Karimi proposed a method of independent control of vehicle height and air spring stiffness based on IASS [13]. In 2018, Li proposed the cooperative control of interconnection and damping for lateral interconnected air suspension based on the multiagent game theory [14]. In 2019, Sun proposed a coordinated game control of interconnected air suspension and damping [15]. According to the above references, the research focus of IASS cooperative control is mostly on pairwise interaction, especially between interconnection mode and damping. However, the IASS actually contains three controllable structures. Therefore, it is necessary to formulate a new control method to realize the cooperative control among the three controllable structures, to give full play to the advantageous performance of IASS.

As can be seen from Figure 2, the MPC controller solves the optimal target $u(t)$ according to the external input information $x(k)$ and $u(k)$ and then transmits it to the system. At the same time, the system simplifies the real-time state information $y(t)$ by the observer and transmits it to the MPC controller, to continuously optimize the optimal target $u(t)$. Relevant scholars designed MPC controller to solve the optimal target suspension force of traditional air suspension in 2020 [16]. In the paper, MPC controller will be designed to solve the optimal target suspension force of new interconnected air suspension.

As can be seen from Figure 3, deliberate agents perceive the external environment and combine it with their own internal states, knowledge base, and mission objectives and then output action execution to actuators finally. In recent years, relevant scholars have applied the agent theory to the traditional air suspension, but it is limited to the single control of damping and vehicle height [17, 18]. In the paper, three deliberate agents corresponding to vehicle height, damping, and interconnection mode are established to realize the cooperative control between them by their own energy consumption and sensing the optimal target suspension force solved by the external MPC controller.

In this study, the interconnected air suspension is taken as research object. The charging and discharging operation of the conventional IASS vehicle height system and the interconnection operation of the air spring will cause both inflation and deflation of the same air spring, which will lead to unnecessary loss of energy consumption, so a cooperative control system based on MPC and multiagent theory is well constructed to achieve a coordination between the control of the three controllable structures in IASS. It can effectively realize the cooperative control between controllable structures in IASS, especially vehicle height and interconnection, to reduce the charging and discharging frequency. At the same time, the ride comfort and handling stability of the vehicle are improved on the premise of reducing energy consumption.

2. IASS Vehicle Model Establishment and Test Verification

2.1. Establishment of the Vehicle Dynamic Model. The whole vehicle model is simplified into the following seven degrees of freedom [19]: the vertical vibration of the unsprung mass and the roll, pitch, and vertical vibration of the sprung mass. The vehicle model is shown in Figure 4.

According to vehicle dynamics, the 7-DOF vehicle model can be expressed as follows:

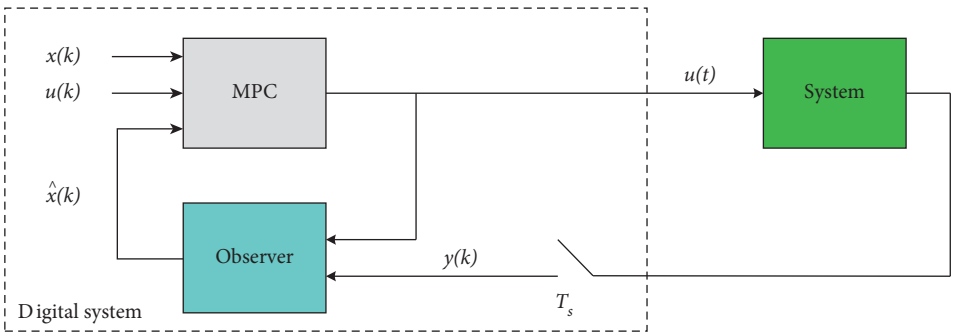

Figure 2: MPC control flow.

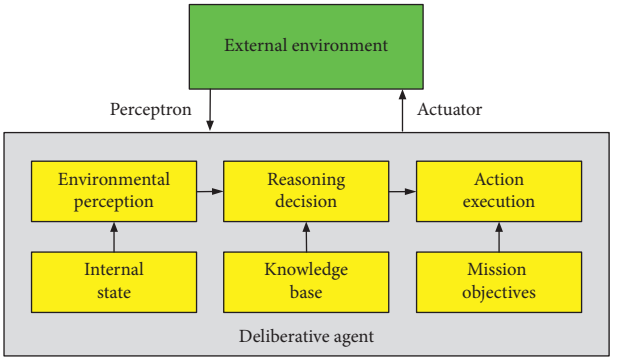

Figure 3: Architecture of the deliberate agent.

$$\begin{cases} F_i = F_{si} + F_{di}, \\ f_{d1} = Z_{t1} - \left(Z_b - l_f\theta + 0.5\varphi B_f\right), \\ f_{d2} = Z_{t2} - \left(Z_b - l_f\theta - 0.5\varphi B_f\right), \\ f_{d3} = Z_{t3} - \left(Z_b + l_r\theta + 0.5\varphi B_f\right), \\ f_{d4} = Z_{t4} - \left(Z_b + l_r\theta - 0.5\varphi B_f\right), \end{cases} \tag{1}$$

where M_b is the sprung mass, kg. Z_b is the vertical displacement at the position of center of gravity of sprung mass, m. F_i is the suspension force at the vehicle position i, N, $i \in$(fl, fr, rl, rr). F_{si} is the air spring force at the vehicle position i, N. F_{di} is the damping force at the vehicle position i, N. I_r is the sprung mass moment of inertia around X-axis, kg.m^2. θ is the sprung mass roll angle around X-axis, rad. I_p is the sprung mass moment of inertia around the Y-axis, kg.m^2. φ is the sprung mass roll angle around Y-axis, rad. l_f and l_r are distances from the center of mass to front and rear axles of the vehicle, m. B_f and B_r are front and rear tracks, m. M_{ti} is the unsprung mass at position i of each wheel, kg. Z_{ti} is the vertical displacement of each unsprung mass, m. K_t is the vertical wheel stiffness, N/m. q_i is the vertical excitation of pavement at the position of four wheels, m. f_{di} is the suspension travel at the vehicle position i.

2.2. Establishment of the Air Spring Model. In the working process, the air inside air springs can be taken as a variable mass open-ended adiabatic system, according to the first law of thermodynamics [20]:

$$P\left(\frac{V}{m}\right)^{\kappa} = C, \tag{2}$$

where P is the gas pressure in the air spring, Pa. V is the volume of the air spring, m^3. m is the mass of gas in the air spring, kg. κ is the adiabatic index, and in this study, $\kappa = 1.4$.

Suppose P_{i0}, V_{i0}, and m_{i0} are the initial air pressure, initial volume, and initial mass of the air spring, respectively, then at any time, the internal gas of the air spring meets the following requirements:

$$P_i\left(\frac{V_i}{m_i}\right)^{\kappa} = P_{i0}\left(\frac{V_{i0}}{m_{i0}}\right)^{\kappa}. \tag{3}$$

The instantaneous air pressure P_i and instantaneous volume V_i of the air spring are obtained by the deformation of the above formula:

$$\begin{aligned} P_{i0} &= P_0\left(\frac{m_i V_{i0}}{m_{i0} V_i}\right)^{k}, \\ V_i &= V_{i0} - \frac{\mathrm{d}V_i}{\mathrm{d}h} d, \end{aligned} \tag{4}$$

where dV_i/dh is the volume change rate of gas chamber, m^3/m; d is the shape variable of air spring, m.

The product of the internal air pressure in the air spring chamber and the effective cross-sectional area value is equal to the vertical spring force:

$$F_s = \left(P_1 - P_0\right) A_1, \tag{5}$$

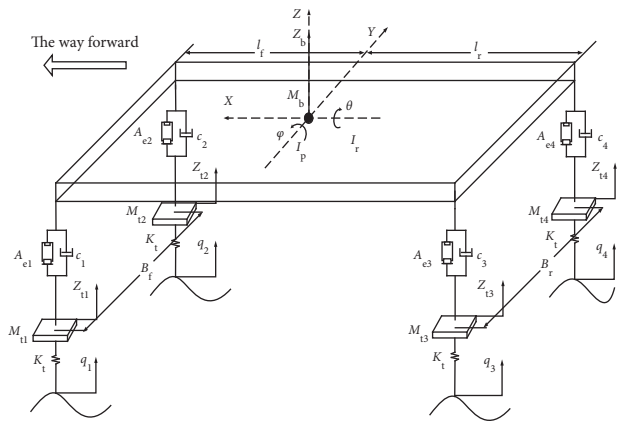

Figure 4: Establishment of the vehicle model.

where F_s is the vertical spring force, N; A_1 is the effective cross-sectional area, m^2; P_0 is atmospheric pressure, Pa; and P_1 is the internal pressure of the air chamber, Pa.

The formula of effective cross-sectional area $A_1$of air spring is as follows:

$$A_1 = -1.6 \times 10^{-8} d^3 - 2.7 \times 10^{-7} d^2 - 3.5 \times 10^{-6} d + 9.1 \times 10^{-3}. \quad (6)$$

Finally, the specific vertical spring force of air spring F_s is as follows:

$$F_s = \left[P_{i0} \left(\frac{m_i V_{i0}}{m_{i0} \left(V_{i0} - \mathrm{d}V_i / \mathrm{d}h \right) d} \right) \right] \times \left(-1.6 \times 10^{-8} d^3 - 2.7 \times 10^{-7} d^2 - 3.5 \times 10^{-6} d + 9.1 \times 10^{-3} \right). \quad (7)$$

Through the above mathematical analysis of the air spring model, the Simulink module is established, as shown in Figure 5.

2.3. Establishment of the Interconnected Pipeline Model. There are two main effects of the interconnected pipeline on gas mass flow: the throttling effect and the hysteresis effect. Therefore, the interconnected pipeline can be taken as the combination of a throttle orifice and a pipeline with a hysteresis effect.

When the gas flows through the orifice, due to the effect of fluid viscosity and mass inertia, the gas mass flow rate can be expressed as [21] follows:

$$\dot{m}(0,t) = \begin{cases} S_e \dfrac{\pi}{4} D^2 P_u \sqrt{\dfrac{1}{\mathrm{RT}_u} \dfrac{2\kappa}{\kappa - 1} \left[\left(\dfrac{P_d}{P_u} \right)^{2/\kappa} - \left(\dfrac{P_d}{P_u} \right)^{\kappa + 1/\kappa} \right]}, & \dfrac{P_d}{P_u} > 0.528, \\ S_e \dfrac{\pi}{4} D^2 P_u \left(\dfrac{2}{\kappa + 1} \right)^{1/\kappa + 1} \sqrt{\dfrac{1}{\mathrm{RT}_u} \dfrac{2\kappa}{\kappa - 1}}, & \dfrac{P_d}{P_u} \le 0.528, \end{cases} \quad (8)$$

where S_e is the flow coefficient, 0.62. D is the inner diameter of the interconnection pipeline, mm. P_u is the upstream gas pressure, Pa. R is the ideal gas constant, kJ (kmol.K). T_u is the upstream gas temperature, K. P_d is the downstream gas pressure, Pa.

Due to the limitation of gas flow rate, there is a delay in the response of gas mass flow rate at the outlet and inlet of interconnected pipeline. Therefore, the variation of gas mass flow rate at different positions of interconnected pipeline with time can be expressed as [21]follows:

$$\dot{m}(L,t) = \begin{cases} 0, & t < \dfrac{L}{v_c}, \\ \dot{m}\left(0, t - \dfrac{L}{v_c} \right) \cdot e^{-\left(R_t R T_d / 2 P_d \right) L / v_c}, & t \ge \dfrac{L}{v_c}, \end{cases} \quad (9)$$

where L is the length of the interconnection pipeline, m. v_c is the sound speed, which is 340 m/s in this study. R_t is the resistance coefficient on the inner wall of interconnected pipelines.

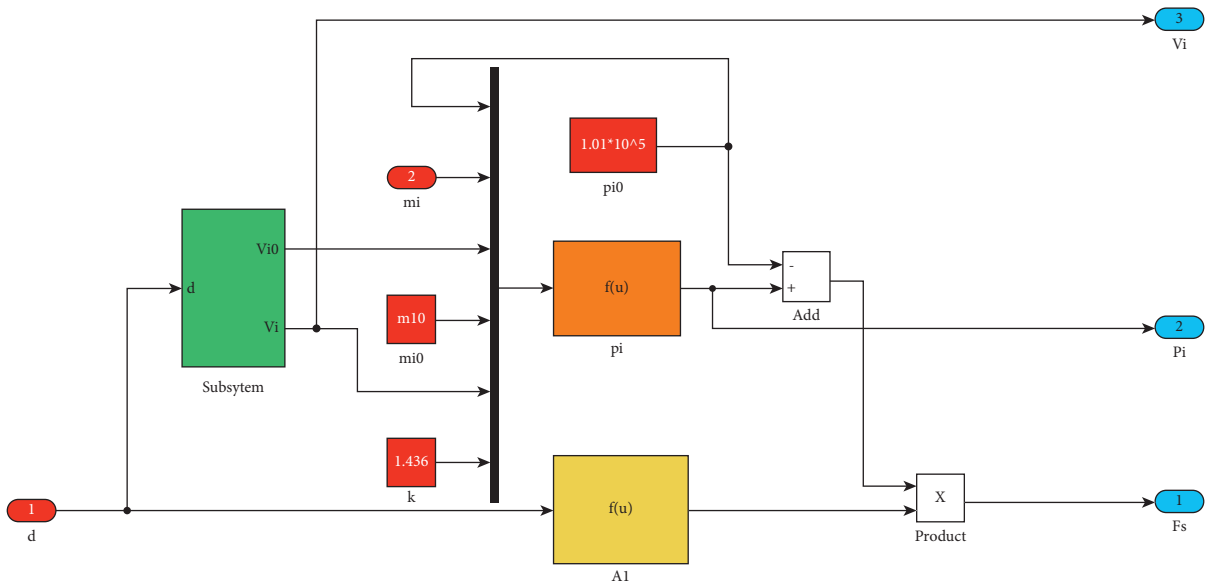

Figure 5: Simulink module of air spring.

2.4. Establishment of Interconnected Air Suspension. The air springs at the front left, front right, rear left, and rear right of the chassis are marked as 1, 2, 3, and 4, the mass airflow from 2 to 1 is recorded as $\dot{m}_{21}$, and the mass airflow from 3 to 1 is recorded as $\dot{m}_{31}$, and then, the mass air $m_1$is [22] as follows:

$$m_1 = m_{10} + \int_0^t \dot{m}_{21}\mathrm{d}t + \int_0^t \dot{m}_{31}\mathrm{d}t, \tag{10}$$

where m_{10} is the initial gas mass of 1, kg.

According to the above principle, the gas mass of other air springs derived from this type is as follows:

$$\begin{cases} m_1 = m_{10} + \int_0^t \dot{m}_{21}\mathrm{d}t + \int_0^t \dot{m}_{31}\mathrm{d}t, \\ m_2 = m_{20} + \int_0^t \dot{m}_{42}\mathrm{d}t + \int_0^t \dot{m}_{12}\mathrm{d}t, \\ m_3 = m_{30} + \int_0^t \dot{m}_{43}\mathrm{d}t + \int_0^t \dot{m}_{13}\mathrm{d}t, \\ m_4 = m_{40} + \int_0^t \dot{m}_{34}\mathrm{d}t + \int_0^t \dot{m}_{24}\mathrm{d}t. \end{cases} \tag{11}$$

Combined with the above analysis formula for air mass flow calculation, the interconnected air suspension module established in Simulink environment is shown in Figure 6.

2.5. Validation of Simulation Model. The test vehicle is a 22-seat medium-sized passenger car produced by the Nanjing Jinlong, as shown in Figure 7. Considering that the test vehicle is too heavy to carry out a bench test, road test is adopted instead for verification. The test vehicle passes through the speed hump at a certain speed, and the accuracy of the model is verified by comparing the collected information with the response of the model. During the driving process of the vehicle, each sensor transmits the collected information to the interconnected drive module. The interconnected drive module controls the opening and closing of the solenoid valve to adjust the ride comfort and handling stability of the vehicle when necessary. Specifications of the model car are shown in Table 1 [23].

According to surveying and mapping results of the speed hump used in the test, the cross-sectional area of the speed hump is determined to be approximated circular arc shape, as shown in Figure 8.

The intersection point between the left side of the outer contour of the speed hump and the ground is taken as coordinate origin, and the cross section of the road surface is taken as X-axis, and the coordinate system is established. The corresponding speed hump excitation can be written as follows:

$$q(t) = \sqrt{\frac{w^2 + 4h^2}{8h} - \left(vt - \frac{w}{2}\right)^2} - \frac{w^2 - 4h^2}{8h} \quad \left(0 \le t \le \frac{w}{v}\right), \tag{12}$$

where v is the vehicle speed, m/s. w is the width of the speed hump, m. h is the height of the speed hump, m.

The test site is a straight asphalt road, and the test and simulation results are shown in Figure 9.

As can be seen from Figure 9, the acceleration test result of the front left side of the vehicle is consistent with the simulation. It can be seen that the peak value of sprung mass acceleration is about 7 m/s^2 under simulation and about 6 m/s^2 under real test. The peak value of the unsprung mass acceleration is about 35 m/s^2 and 30 m/s^2 under simulation and real test, respectively. Considering the friction between rubber bushing and suspension joint, as well as engine excitation and other factors, the response error at each moment is within an acceptable range.

For the rollover characteristics of the vehicle, considering the safety of experimenters and other factors, the artificial vibration method is used to verify the rollover characteristics of the vehicle. The vehicle is stationary on the flat road, and the artificial excitation is given. The vehicle is

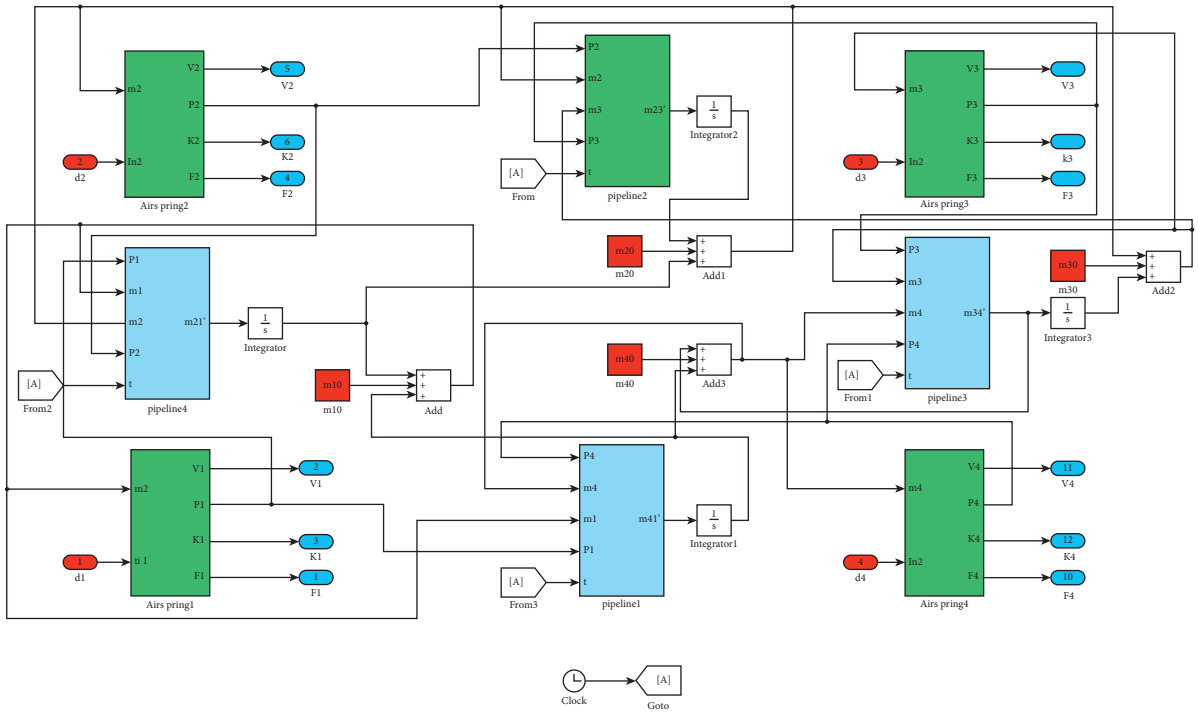

Figure 6: Simulink module of interconnected air suspension.

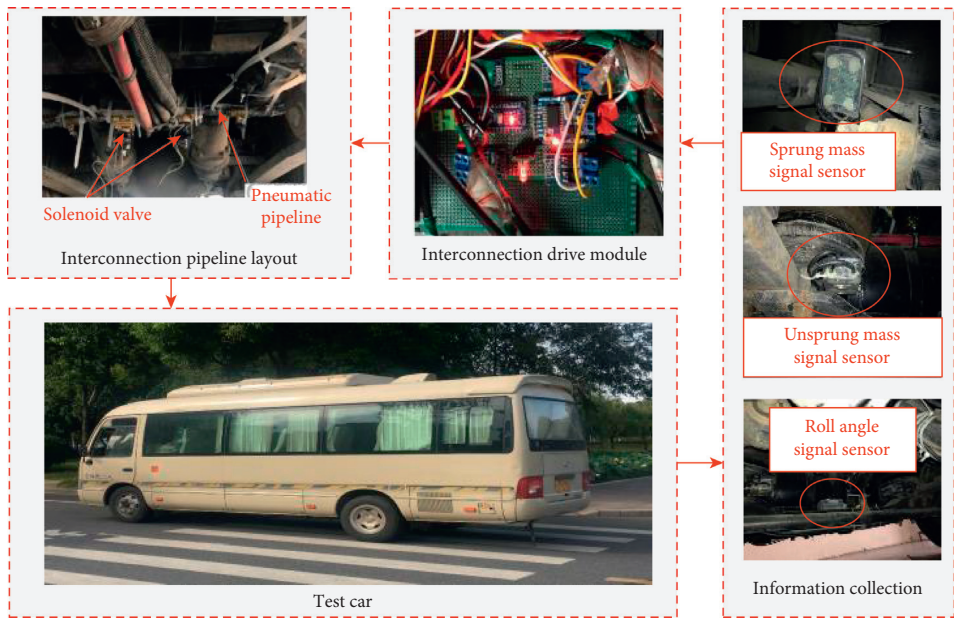

Figure 7: Schematic diagram of the test system.

shaken laterally. The angular accelerator is placed at the vehicle center of mass, and its body roll angle velocity is recorded [24]. The results of the experiment and simulation are compared as shown in Figure 10.

It can be seen from Figure 10 that the attenuation trend of vehicle rollover angular frequency and amplitude in test scenario is consistent with simulation, and the response error at each time is within an acceptable range. This indicates that the simulation model can closely reflect the rollover characteristics of the test vehicle.

3. Control System Design

As can be seen from Figure 11, firstly, after the vehicle is excited by the road, the state information $y(t)$ generated is simplified by the observer and transmitted to the MPC controller. The suspension force output by the MPC is constrained by the suspension force to form the optimal target suspension force $u(k)$. Secondly, the three controllable structures (interconnection mode, vehicle height, and damping) are regarded as three deliberative agents. The

Table 1: Specifications of the model car.

Parameter name and unit	Value	Parameter name and unit	Value
Unloaded sprung mass Mb (kg)	4500 kg	Unloaded unsprung mass of front axle M_{uf} (kg)	300 kg
Unloaded unsprung mass of rear axle M_{ur} (kg)	500 kg	The inertia of sprung mass about X-axis I_r (kg·m^2)	3757 kg m^2
The inertia of sprung mass about Y-axis I_p (kg·m^2)	7391 kg m^2	Height of sprung mass centroid h_{cg} (m)	1.1 m
Distance from the body centroid to front axle l_f(m)	2.665 m	Distance from the body centroid to rear axle l_r (m)	1.27 m
Tire stiffness K_t (kN/m)	210 kN/m	Wheelbase L(m)	3.935 m
Front track width B_f(m)	1.665 m	Rear track width B_r(m)	1.525 m
The damping force of shock absorber in extension stroke F_1 (N)	2915 N	The damping of shock absorber in compression stroke F_2 (N)	1335 N

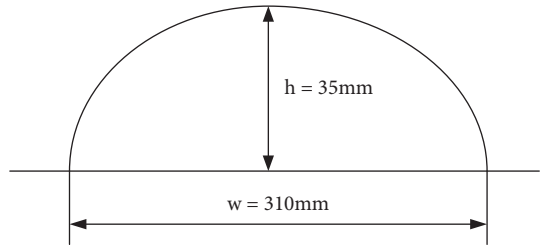

Figure 8: Transect of the speed hump.

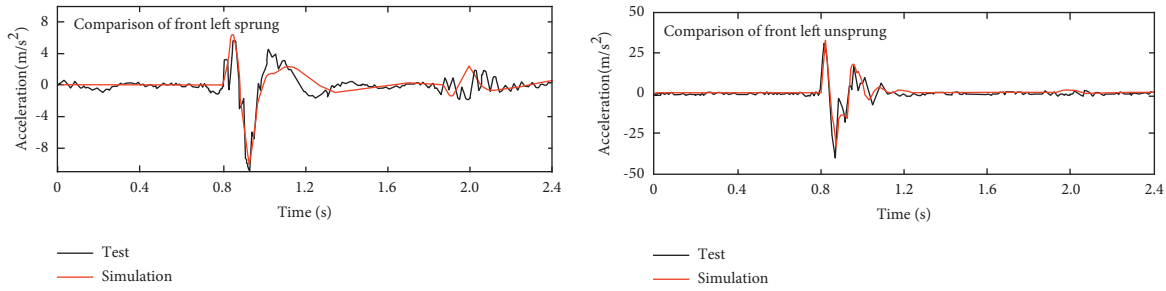

Figure 9: Vertical acceleration between front left sprung mass and front left unsprung mass.

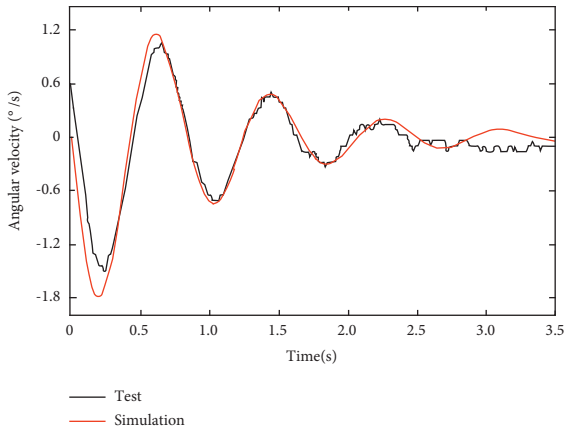

Figure 10: Comparison of roll angular velocity.

optimal target suspension force is distributed according to their internal energy consumption. Finally, the damping agent acts on the damper to output the damping force F_D, and the vehicle height agent and the interconnected agent act on the air spring to output the air spring force F_S. The output damping force F_D and air spring force F_S feedback act on the vehicle to improve the vehicle performance.

3.1. Design of the MPC Controller

3.1.1. Model Discretization. Since MPC uses discrete-time models to solve the optimization problems, it is necessary to discretize the existing continuous-time state equation using sampling time T_s and zero-order holder. The discrete state equation is written as follows [16]:

$$\begin{aligned} \begin{cases} x[k+1] &= A_d x[k] + B_{du} u[k] + B_{d\omega} \omega[k], \\ y[k] &= C_d x[k] + D_{du} u[k] + D_{d\omega} \omega[k], \end{cases} \\ A_d = e^{AT_s}, \\ \begin{bmatrix} B_{du} \\ B_{d\omega} \end{bmatrix} = A^{-1} (A_d - I) \begin{bmatrix} B_u \\ B_\omega \end{bmatrix}, \\ C_d = C, \\ D_d = D. \end{aligned} \tag{13}$$

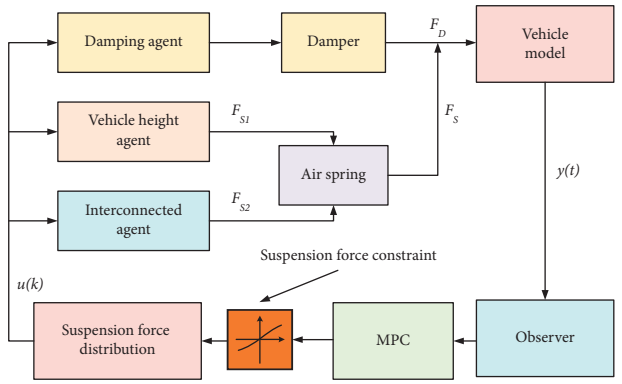

Figure 11: Control flow diagram.

The following MPC controller design will be based on the discrete state equation.

3.1.2. Costs and Constraints. The control objective of the MPC controller is to reduce the acceleration at four corners of sprung mass, tire dynamic load, and suspension breakdown probability, and quadratic form is written as the cost function of the controller.

The control target W of the controller is the algebraic sum of the product of sprung mass acceleration, suspension travel, and tire deformation and their respective weight coefficients ρ_s, ρ_{fd}, and ρ_{um}. Combined with the discrete-time domain state equation of (7), W can be expressed as follows:

$$W = C_{dW}x[k] + D_{duW}u[k] + D_{d\omega W}\omega[k], \tag{14}$$

where $\boldsymbol{C_{dW}}$, $\boldsymbol{D_{duW}}$, and $\boldsymbol{D_{d\omega W}}$ are state matrices of W, respectively.

In addition to the above control objectives, the control cost to achieve objectives is often taken into account to limit the energy consumption of the system. Therefore, the cost function of the whole MPC controller can be written as follows:

$$\begin{aligned} J &= x[N]^T Px[N] + \sum_{i=0}^{N-1}\left\{W[i]^T Q_W W[i] + u[i]^T R_W u[i]\right\}, \\ Q_W &= \begin{bmatrix} \rho_s I_4 & 0 & 0 \\ 0 & \rho_{f\,d} I_4 & 0 \\ 0 & 0 & \rho_{um} I_4 \end{bmatrix}, \\ R_W &= \rho_u I_4, \end{aligned} \tag{15}$$

where ρ_u is the weight coefficient of control quantity u and $\boldsymbol{P}$ is the weight matrix of the terminal state. Q_w is the state weight matrix, and R_w is the input weight matrix. For this system, its terminal state is set to 0, so the matrix $\boldsymbol{P}$ term can be ignored.

The control variable u of the MPC controller designed in this study is suspension force, and the final suspension force F is composed of adjustable damping force F_D produced by an adjustable damper, air spring force F_I produced by switched interconnection mode, and air spring force F_H produced by changed vehicle height.

$$F = F_D + F_I + F_H. \tag{16}$$

There are some constraints on the force produced by each component. Therefore, this restriction should be considered in the form of constraints when designing the MPC controller to ensure that optimal control variable is within the range of suspension capacity.

For a single damper, the damping force F_{damper} is related to the relative velocity between sprung mass and unsprung mass.

$$F_{\text{damper}} = c\left(\dot{Z}_s - \dot{Z}_u\right) = c\dot{f}_d. \tag{17}$$

If the damping coefficient $c \in [c_{\min}\ c_{\max}]$, then for the whole damper, the constraint of damping force F_{damper} can be expressed as follows:

$$\begin{cases} c_{\max}\dot{f}_d \le F_{\text{damper}} \le c_{\min}\dot{f}_d, & \dot{f}_d \le 0, \\ c_{\min}\dot{f}_d \le F_{\text{damper}} \le c_{\max}\dot{f}_d, & \dot{f}_d > 0. \end{cases} \tag{18}$$

If damping of the system is regarded as the combination of uncontrollable part $c_{\min}$ and controllable part [0 c_{max}-c_{min}], then for the whole vehicle, the constraint of damping force F_D on the controllable part of each damper is as follows:

$$\begin{cases} 0 \ge F_{Di} \ge (c_{\max} - c_{\min})\dot{f}_{\text{d}}, & \dot{f}_{\text{d}} \le 0, \\ 0 \le F_{Di} \le (c_{\max} - c_{\min})\dot{f}_{\text{d}}, & \dot{f}_{\text{d}} > 0. \end{cases} \tag{19}$$

Assuming that air springs at the front left and front right positions of the vehicle are fully open, and the air pressure of the front left air spring P_{fl} is greater than that of the front right air spring P_{fr}, the mass of gas flowing into the air spring is considered to be positive, and the mass of gas flowing out of the air spring is considered to be negative. The force change in the air spring pressure on both sides due to interconnection is as follows:

$$\begin{cases} F_{\max}^{Ifl} = \Delta P_{Ifl}[k]S_{0fl}, \\ F_{\min}^{Ifr} = \Delta P_{Ifr}[k]S_{0fr}. \end{cases} \tag{20}$$

At the same time, if the interconnection mode is closed, the change in force generated by the interconnection of two air springs is zero at the current moment. Then, under such conditions, the constraint of the change in force generated by the interconnection of front left and front right air springs can be written as follows:

$$\begin{cases} 0 \le F_{Ifl} \le F_{\max}^{Ifl}, \\ P_{fl} > P_{fr}, \\ F_{\min}^{Ifr} \le F_{Ifr} \le 0. \end{cases} \tag{21}$$

Similar to the constraint form of interconnection mode, the constraint of body height adjustment on the change in air spring force can also be written as follows:

$$\Delta P_{Hi}[k]S_{0i} \le F_{Hi} \le \Delta P_{Hi}[k]S_{0i}. \tag{22}$$

Combined with the above three constraints, the constraint of vehicle control variable u can be expressed as the intersection of the three.

3.1.3. Generation of the Cost Strategy for Multiagent Energy Consumption. In the whole vehicle system, the suspension force produced by each agent has the same influence on the whole vehicle, but the energy consumption of each agent is different. Therefore, in the optimal suspension force distribution, the operating cost of each agent should be considered.

For a damper, assuming that V_D denotes the supply voltage and I_D denotes the current, they can be obtained through relevant sensors, the operating cost of the damping agent during each sampling interval is as follows:

$$J_d = \sum_{i=1}^{4} \int_0^{T_s} V_d I_d \mathrm{d}t, \tag{23}$$

where $i \in (1,2,3,4)$ represents the dampers at four locations *fl*, *fr*, *rl*, and *rr,* respectively.

Assuming that the consumption of the control system is involved in cost function and the power of the interconnected solenoid valve is denoted by E_I, the operating cost function of the interconnected agent during each sampling interval is as follows:

$$\begin{aligned} J_I(t_i) &= \sum_{i=1}^{4} \int_0^{t_i} E_I \mathrm{d}t \\ &= E_I \sum_{i=1}^{4} t_i, \end{aligned} \tag{24}$$

where $i \in (1, 2, 3, 4)$ represents four solenoid valves in the interconnected pipelines, respectively.

Assuming that E_H denotes the power of the pneumatic solenoid valve, the operating cost of the pneumatic solenoid valve for the vehicle height adjustment agent during each sampling interval is as follows:

$$\begin{aligned} J_{H_v}(t_{ci}, t_{di}) &= \sum_{i=1}^{4} \left(\int_0^{t_{ci}} E_H \mathrm{d}t + \int_0^{t_{di}} E_H \mathrm{d}t \right) \\ &= E_H \sum_{i=1}^{4} (t_{ci} + t_{di}), \end{aligned} \tag{25}$$

where $i \in (1,2,3,4)$ is the air springs in the pneumatic pipelines at four locations *fl*, *fr*, *rl*, and *rr,* respectively.

Meanwhile, in the process of air compression, the power of the compressor P can be calculated according to the following formula:

$$P = \frac{\kappa}{\kappa - 1} \mathrm{RT} q \left[\left(\frac{P_1}{P_0} \right)^{\kappa - 1/\kappa} - 1 \right], \tag{26}$$

where P_1 is the absolute pressure at the discharge port of the air compressor, P_0 is the absolute pressure at the inlet port of the air compressor, and q is gas mass flow through the air compressor.

K is as follows:

$$K = \frac{\kappa}{\kappa - 1} \mathrm{RT} \left[\left(\frac{P_1}{P_0} \right)^{\kappa - 1/\kappa} - 1 \right]. \tag{27}$$

For the intake process, P_1 represents the pressure of the high-pressure tank, and P_0 represents the air spring pressure; for the discharge process, P_1 represents the air spring pressure, and P_0 represents the atmospheric pressure.

Thus, the cost function of gas mass variation inside the air springs during the process of charging and discharging is as follows:

$$J_{Ha}(t_{ci}, t_{\mathrm{d}i}) = \sum_{i=1}^{4} \left(\int_0^{t_{ci}} K_c q_{ci} \mathrm{d}t + K_d q_{\mathrm{d}i} \mathrm{d}t \right). \tag{28}$$

The total operating cost of vehicle height agent during the sampling interval can be written as follows:

$$J_H(t_{ci}, t_{\mathrm{d}i}) = J_{Hv}(t_{ci}, t_{\mathrm{d}i}) + J_{Ha}(t_{ci}, t_{\mathrm{d}i}). \tag{29}$$

It can be concluded that the operating cost value of vehicle height agent is the highest, followed by interconnected agent, and the operating cost value of damping agent is the lowest.

The regular pattern of how three agents change their intention to cooperate is shown in Figure 12, where A corresponds to damping agent, B corresponds to interconnected agent, and C corresponds to vehicle height agent. $A < B < C$ when it comes to energy consumption cost.

When the optimal suspension force is too large, the three agents tend to cooperate with each other to jointly distribute the optimal suspension force.

When the optimal suspension force is reduced to A and B can be completed together, as the agent with the highest energy consumption, C agent's cooperation request will be rejected by A and B. Finally, agent C is closed, and A and B jointly distribute the optimal suspension force to reduce energy consumption.

When the optimal suspension force is further reduced to the extent that agent A can bear it alone, agents B and C are closed, and agent A bears the optimal suspension force alone, further reducing the energy consumption of the system.

3.1.4. Analysis of Cooperative Control Effect Based on the MPC and the Multiagent Theory. To verify the control method, the simulation is carried out in the Simulink environment of MATLAB. Because the research object is a new suspension structure, to ensure the safety, the speed is generally controlled at 30 to 40 km/h during the real vehicle test. Therefore, the similar speed is set during the simulation, which corresponds to the real vehicle test. The paper is set to 10 m/s.

When the vehicle velocity is 10 m/s, the control effect under cooperative control and noncooperative control with different road conditions is compared. The results are shown

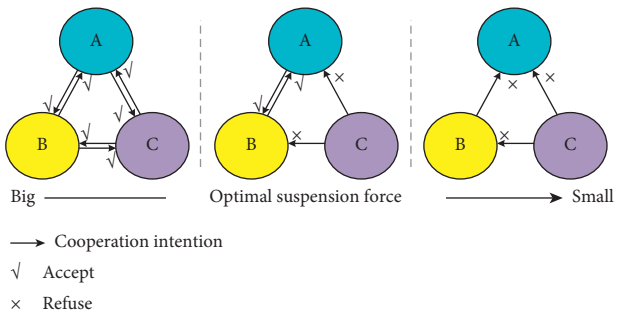

Figure 12: Change in agents' cooperation intentions.

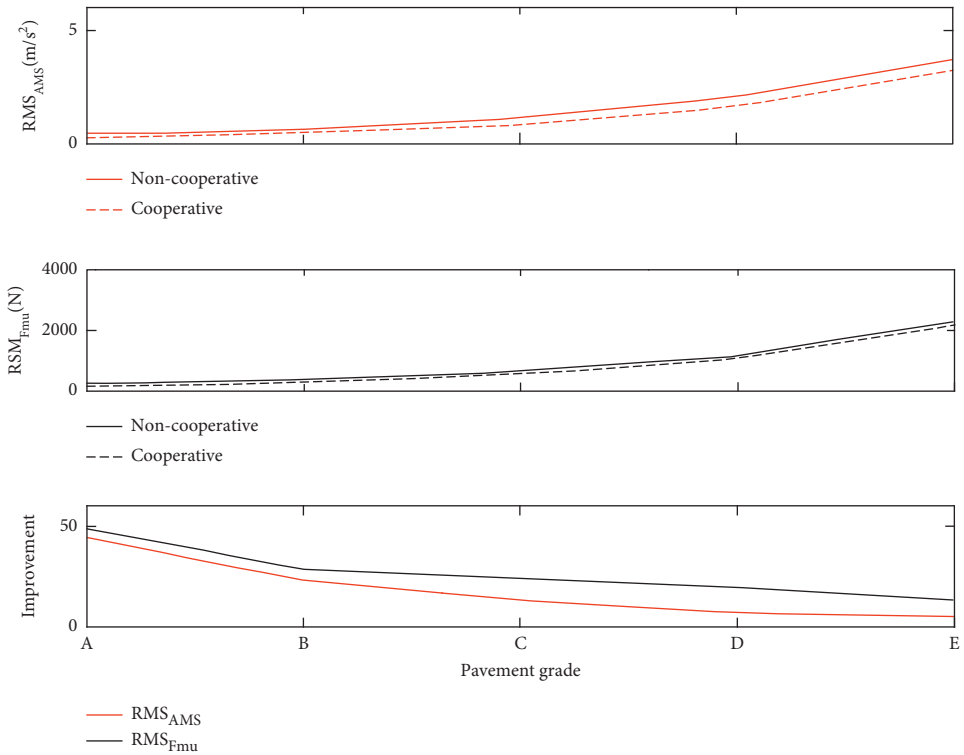

Figure 13: Influence of cooperative control and noncooperative control.

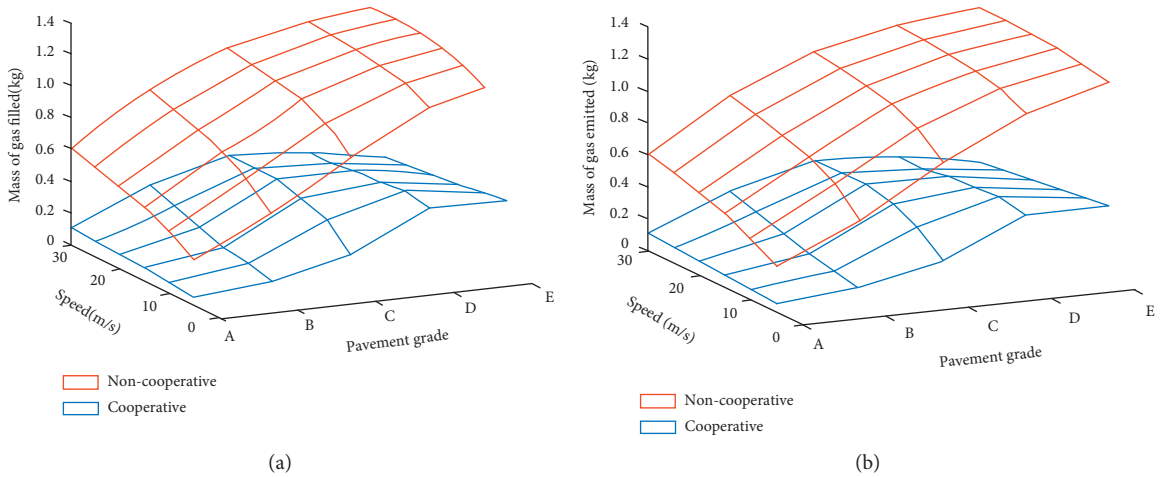

Figure 14: Energy consumption of cooperative control and noncooperative control. (a) Mass of gas filled. (b) Mass of gas emitted.

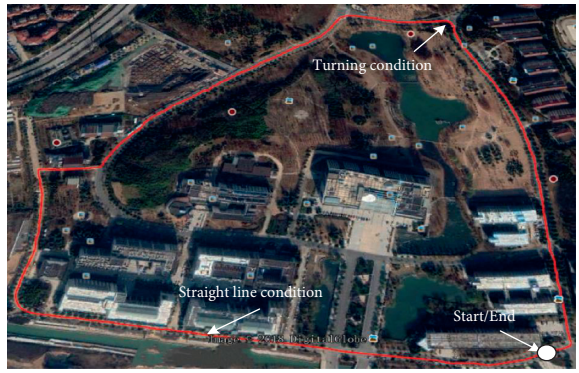

Figure 15: Road map of the test.

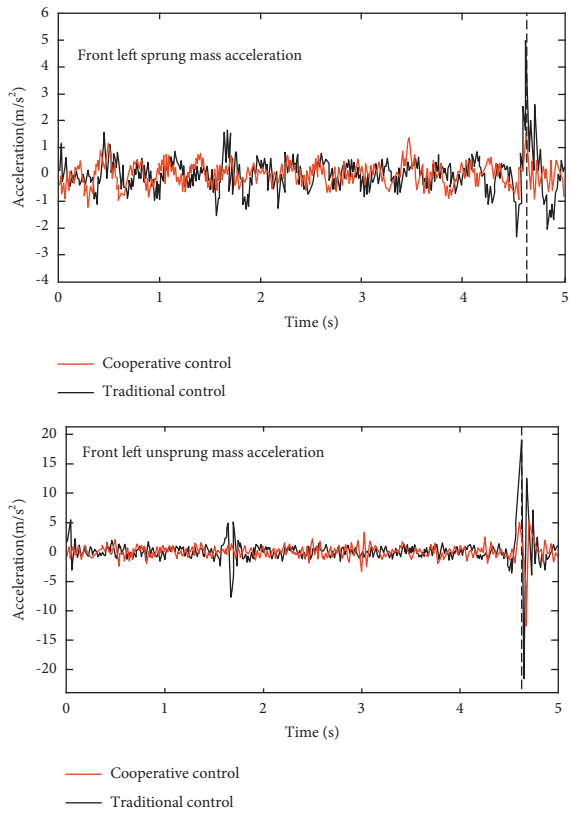

Figure 16: Segment acceleration of front left sprung and unsprung mass.

in Figure 13. It clearly shows that the improvement rate of RMS value of sprung mass acceleration and tire dynamic load is 10%–49% and 4%–46%, respectively, which proves that the three controllable components in the interconnected air suspension system can work cooperatively under the cooperative control method.

In the process of body height adjustment, energy consumption of charging and discharging process is enormous. In this study, the gas mass flowing into or out of the air spring in unit time for adjusting body height is selected as an evaluation index of system energy consumption. It can be seen from Figure 14 that the gas mass during the process of charging and discharging is significantly reduced when a cooperative control strategy is adopted, and energy consumption of the whole system is greatly reduced compared with that using a noncooperative control strategy.

3.2. Real Vehicle Test Verification. To verify the control effect of the cooperative control method on interconnected air suspension, the corresponding real vehicle test is carried out, and the test road segments are shown in Figure 15. The total length of the selected route is about 2.2 km. Two working conditions, straight-driving condition and steering condition, are covered. Two control strategies, traditional control and cooperative control, are adopted. The test speed is 30 km/h.

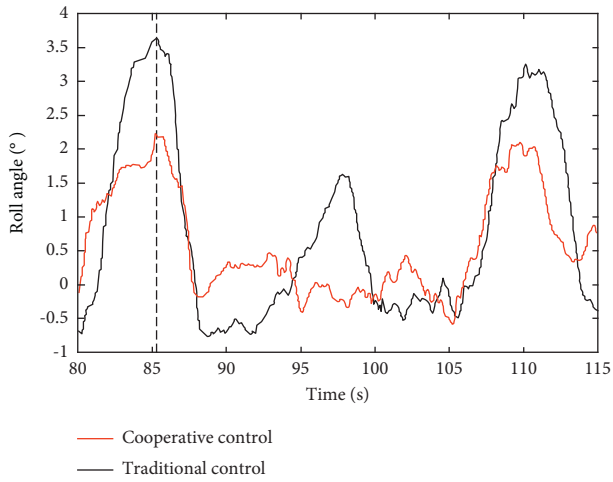

Figure 17: Segment vehicle roll angle response.

As for the traditional control, the damper adopts the classical skyhook control strategy, the interconnection control system adopts the imitation skyhook interconnection state control strategy, and the vehicle height adjustment system adopts the PID-PWM control strategy [25].

The segment of the front left sprung mass acceleration and unsprung mass acceleration under straight-driving conditions is shown in Figure 16. It can be seen that the peak value of sprung mass acceleration is about 5 m/s^2 under traditional control strategy and about 1.5 m/s^2 under cooperative control strategy, which is reduced by 70%. The peak value of the unsprung mass acceleration is about 20 m/s^2 and 5 m/s^2 under traditional control and cooperative control, respectively, which is reduced by 75%. The results prove that cooperative control can significantly improve the ride comfort of the vehicle.

The segment of roll angle response understeering condition is shown in Figure 17. It can be seen that understeering condition, the body roll is restricted using a cooperative control strategy. Compared with using a traditional control strategy, the peak value of the body roll angle is reduced by about 40%. To a certain extent, it proves that the cooperative control system can improve the handling stability of the vehicle.

4. Conclusions

Aiming at the defects of conventional IASS in energy consumption and control strategy, a cooperative control system based on MPC and agent theory is designed to achieve coordination between the controls of the three controllable structures in IASS. Each agent in the system can allocate the suspension force generated by the MPC controller according to its own energy consumption cost. It can effectively realize cooperative control on the premise of reducing energy consumption.

Through simulation and real vehicle tests, the control and energy-saving effect of the cooperative control system are verified. Compared with the traditional control method, the sprung mass acceleration is reduced by 70%, the unsprung mass acceleration is reduced by 75% under straight-driving condition, and the body roll angle peak value is reduced by 40% understeering condition. The comprehensive performance of the vehicle during driving is guaranteed.

Data Availability

The data used to support the findings of this study are included within the article.

Conflicts of Interest

The authors declare that they have no conflicts of interest regarding the publication of this study.

Acknowledgments

This work was financially supported by the National Natural Science Foundation of China (no. 51975254).

References

[1] T. Lv, Y. Zhang, and Y. Duan, "Kinematics & compliance analysis of double wishbone air suspension with frictions and joint clearances," *Mechanism and Machine Theory*, vol. 156, pp. 104–127, 2021.

[2] Z. Li, X. Song, X. Chen, and H. Xue, "Dynamic characteristics analysis of the hub direct drive-air suspension system from vertical and longitudinal directions," *Shock and Vibration*, vol. 2021, no. 11, Article ID 8891860, 17 pages, 2021.

[3] C. Yin, D. Zhao, and J. Zhang, "Body height robust control of automotive air suspension system using finite-time approach," *Asian Journal of Control*, vol. 6, 2021.

[4] W. Higginbotham, "Interconnected air suspension," Patent 2988372, USA, 1961.

[5] S. Y. Bhave, "Effect of connecting the front and rear air suspensions of a vehicle on the transmissibility of road undulation inputs," *Vehicle System Dynamics*, vol. 21, no. 1, pp. 225–245, 1992.

[6] G. Dou, W. Yu, and Z. Li, "Sliding mode control of laterally interconnected air suspensions," *Applied Sciences*, vol. 10, no. 12, p. 4320, 2020.

[7] R. Rover, "Purchasing a range rover mark III/L322: details and assistance for purchasing a third generation range rover," 1978, http://www.rangerovers.net/researchl322.htm.

[8] Z. X. Li, Z. Cui, and M. Li, "Modeling of interlinked air suspension and study on its dynamic performance," *Applied Mechanics and Materials*, vol. 494, pp. 163–166, 2014.

[9] X. Xu, L. Sun, Z. Cui, and L. Ju, "Stability analysis of electronically controlled air suspension ride height system based on center manifold method," *Journal of Computational and Theoretical Nanoscience*, vol. 11, no. 2, pp. 385–390, 2014.

[10] W. Yu, *Research on the Cooperative Control Method of Vehicle Interconnected Air Suspension System*, Dissertation of Jiangsu University, Zhenjiang, China, 2020.

[11] S. Wang, L. Chen, and X. Sun, "Analysis of multi-mode switching control model for semi-active air suspension," *Journal of Jiangsu University*, vol. 34, no. 6, pp. 637–642, 2013.

[12] L. Q. Sun and Z. Cui, "Semi-active lateral interconnected air suspension hierarchical control," *Advanced Materials Research*, vol. 1030, pp. 1537–1542, 2014.

[13] P. Eskandary, *Interconnected Air Suspensions with Independent Height and Stiffness Tuning*, Dissertation of Waterloo University, Waterloo, Canada, 2014.
[14] Z. Li, W. Tang, J. Huang, and Y. Lu, "Game control of multi-agent damper system for laterally interconnected air suspension," *Journal of Transportation Engineering*, vol. 18, no. 5, pp. 130–139, 2018.
[15] L. Sun, Y. Lin, G. Geng, Z. Li, and H. Jiang, "Research on switching interconnection modes and game control of interconnected air suspension," *Energies*, vol. 12, no. 17, p. 3218, 2019.
[16] W. Yu and Y. Zhou, "Cooperative control of damping and body height based on model prediction," *Journal of Jiangsu University*, vol. 42, no. 6, pp. 513–519, 2021.
[17] T. Lu and A. Shen, "Research on optimal damping control of air suspension based on agent theory," *Agricultural Equipment & Vehicle Engineering*, vol. 58, no. 12, pp. 5–9, 2020.
[18] H. Jiang, P. Wang, and Z. Li, "Research on air suspension vehicle height intelligent control system based on agent theory," *Journal of Chongqing University of Technology(Natural Science)*, vol. 33, no. 4, pp. 17–25, 2019.
[19] Z. Li, A. Shen, and H Jiang, "Research on multi-agent game control system of an electronic air suspension," *Automotive Engineering*, vol. 42, no. 6, pp. 793–800, 2020.
[20] Z. Zhang, J. Wang, L. Hu, and C. Huang, "Semi-active control of air suspension considering pavement preview information and parametric uncertainty," *Journal of Vibration and Shock*, vol. 39, no. 23, pp. 21–29, 2020.
[21] Z. Li, X. Guan, and H. Jiang, "Research on control of horizontally interconnected air suspension system based on agent theory," *Automotive Engineering*, vol. 41, no. 8, pp. 897–904, 2019.
[22] A. Shen, *Cooperative Control of Laterally Interconnected Air Suspension Based on Multi-Agent Theory*, Dissertation of Jiangsu University, Zhenjiang, Chian, 2020.
[23] X. Guan, *Research on Interconnecting State Control of Laterally Interconnected Air Suspension Based on Agent Theory*, Dissertation of Jiangsu University, Zhenjiang, China, 2019.
[24] H. Li, J. Li, and L. Wang, "Research on the centroid position measurement system of vehicle equipment," *Journal of Machine Design*, vol. 38, no. 7, pp. 96–99, 2021.
[25] L. Ju, *Research on Characteristics of Lateral Interconnected Air Suspension and Control Theory of Simulation Ceiling Interconnection State*, Dissertation of Jiangsu University, Zhenjiang, China, 2016.